Two-Photon Spectroscopy of the Q-Bands of *meso*-Tetraphenyl-Porphyrin and -Chlorin Framework Derivatives

Jordan A. Greco,[†] Sumie Shima,[†] Nicole L. Wagner,[‡] Jason R. McCarthy,[†] Karissa Atticks,[†] Christian Brückner,*[,†] and Robert R. Birge*[,†,‡]

[†]Department of Chemistry, University of Connecticut, 55 North Eagleville Road, Storrs, Connecticut 06269-3060, United States
[‡]Department of Molecular and Cell Biology, University of Connecticut, 91 North Eagleville Road, Storrs, Connecticut 06269-3125, United States

Ⓢ *Supporting Information*

ABSTRACT: The two-photon absorption and excitation spectra in the Q-band region (900−1360 nm) were measured for a number of porphyrinoids, including simple porphyrins (porphin, *meso*-tetraphenyl-porphyrin), chlorins (*meso*-tetra-phenyl-2,3-dimethoxychlorin), and porphyrin and chlorin-like analogues (*meso*-tetraphenyl-porpholactone and *meso*-tetra-phenyl-porpholactol, respectively). These molecules were chosen to provide a series of compounds that differed structurally only in "single points". Vibronic structure is observed in the two-photon spectra for all porphyrinoids investigated, but their relative intensities show distinct differences from the vibronic development observed in the corresponding one-photon spectra. A Franck−Condon analysis provides insight into the observed differences. The calculations also indicate that the two-photon absorptivities are associated primarily with Type I processes involving multiple intermediate states, and that accurate assignment requires a summation over at least 30 intermediate states. The Q-bands of the *meso*-tetraphenyl-2,3-dimethoxychlorin exhibit anomalously high two-photon absorptivities, which we have traced to facile conformational distortion of the chlorin chromophore. Calculations indicated that the relative Q-band absorptivities are sensitive to the phase and magnitude of the chlorin ring distortions.
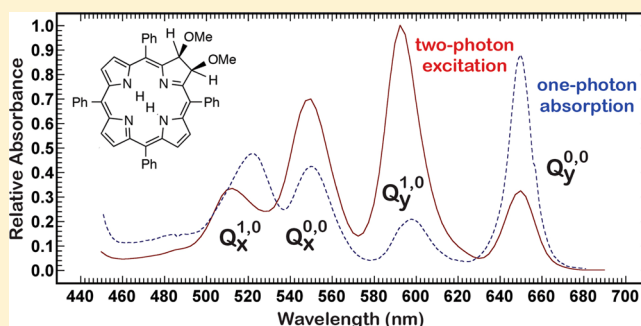
INTRODUCTION

The nonlinear optical properties of porphyrins and related oligopyrrolic compounds have been widely investigated due to their potential utility in medical and optical sensing technologies.[1−9] For instance, the ability of porphyrins and chlorins to generate the highly cytotoxic singlet oxygen ($^1O_2$) upon irradiation with visible light recommends them for use in the photodynamic therapy (PDT) of tumors.[1,10−12] However, a major limitation of one-photon-mediated PDT is associated with the visible wavelengths needed to activate a porphyrin. Blue and green light, the wavelengths absorbed best by regular porphyrins, do not penetrate tissue to any appreciable depths and possess low spatial selectivity due to scatter.[13,14]

Two-photon absorption is a nonlinear optical process that involves the simultaneous absorption of two photons.[15,16] This optical process provides an advantageous alternative for activating porphyrin photosensitizers because it promotes the chromophore into an excited state using the combined energy of two near-infrared (NIR) photons ($\lambda \approx 700{-}1400$ nm), which typically fall in a region where no one-photon absorption exists for the molecule. Importantly, the NIR region also falls within the optical window of biological tissue.[17] While significant effort has been directed toward the design of porphyrins, chlorins, and bacteriochlorins to enhance one-

photon absorption in the NIR domain,[18−24] we focus here on enhancing the two-photon absorptivities of the two lowest-lying singlet states of porphyrin and chlorin analogues. The quadratic dependence of two-photon absorption on laser intensity allows for high spatial resolution of the PDT event and three-dimensional selectivity to target tumors at greater depths.

Porphyrins comprise four pyrrole subunits linked by methine bridges, which yields a closed-conjugated aromatic 18 π-electron system that is cross-conjugated with two β,β'-double bonds (Figure 1). The fully unsaturated aromatic structure is highly planarized and dominates the chemical and physical properties of porphyrins. Electronic properties are highly sensitive to modifications of one (or both) of the β,β'-double bonds.[25,26] Reduction of a β,β'-double bond results in the formation of a chlorin. The addition of *meso*-aryl substituents generally leads to little cross-talk with the porphyrinoid chromophore because *o*-aryl-to-β-hydrogen steric interactions hold the aryl groups in idealized orthogonal orientation with respect to the chromophore;[27] however, distortion to the macrocycle core often permits interaction with *meso*-substitu-
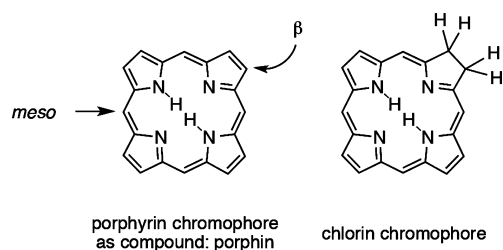
Figure 1. Chromophore structure of porphyrins and chlorins and the naming convention of the *meso-* and *β*-positions.

ents and leads to modulation of the optical properties of these systems.[28]

The entirely unsubstituted porphyrin macrocycle is referred to as porphin (Figure 1). Gouterman's four-orbital model of porphyrins describes the origin of the linear absorption of porphyrins and chlorins by transitions within the two highest occupied molecular orbitals (HOMOs) and the two lowest unoccupied molecular orbitals (LUMOs).[29] The one-photon absorption spectrum of porphin is composed of a Soret band (also called B-band), an intense band found at ~400 nm, and a set of Q-bands between 500 and 650 nm that decrease in intensity with increasing wavelength. Figure 2 demonstrates that the Q_x (570 nm) and Q_y (500 nm) transitions correspond
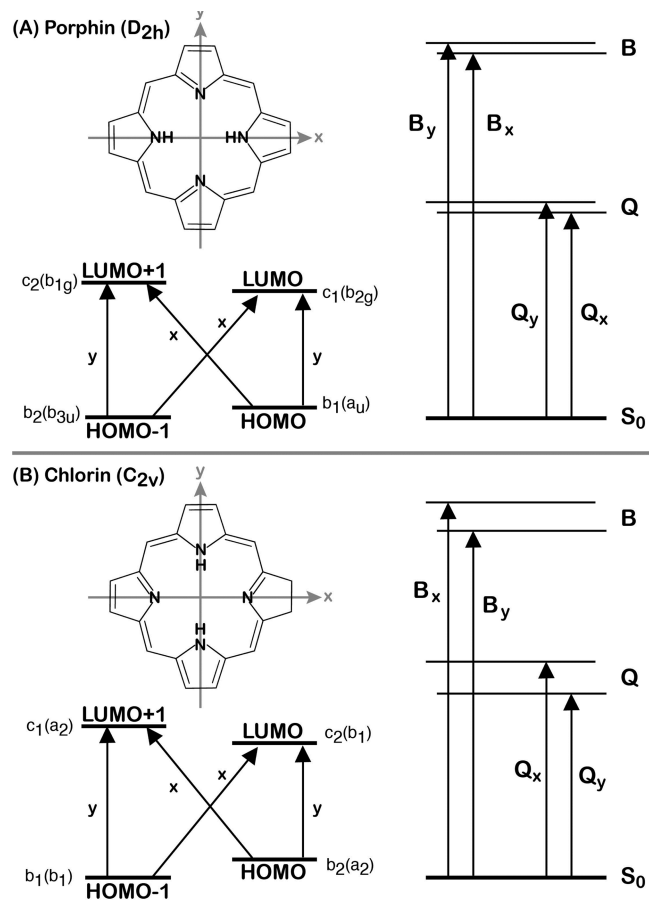
Figure 2. Coordinate systems used to assign the low-lying weakly allowed (Q) bands and the higher energy, strongly allowed Soret (B) bands in porphin (A) and chlorin (B) systems. Note that, unfortunately, the historical assignments create a situation where the lowest Q-band in porphyrins is designated Q_x, whereas the lowest Q-band in chlorins is designated Q_y.

to the *x*- and *y*-polarized transitions.[30] As defined by Gouterman,[29] the *x*-axis runs through the sp^2-hybridized nitrogen atoms, whereas the *y*-axis runs through the sp^3-hybridized nitrogen atoms. The symmetry of the four molecular orbitals (MOs) are also shown in Figure 2.[19,21,22] The electron density of the b_1 and c_2 orbitals are dominated by β,β'-double bonds, and are therefore destabilized upon saturation of the double bond.[31,32] Substitution and/or oxidation of the β,β'-double bond of porphin also reduces the symmetry, which broadens the Soret band due to an increased separation of two degenerate energy levels.[29]

Reduction of the free-base porphyrin to chlorin decreases the symmetry of the chromophore to C_{2v}, generating characteristic chlorin optical spectra.[33−35] The B-band to Q-band ratio and the Q_x to Q_y band ratio are modulated relative to those of porphin. The intensity of the Q-bands depends on mixing with the B-bands, which is proportional to the square of the energy gap between these orbitals.[36] Moreover, the increased conformational flexibility of the chlorin chromophore leads to a broadening of the spectral features, and any nonplanar conformations lead to a general red-shift of the spectra.[25,26] We will adhere to the historical axis labeling convention shown in Figure 2, in which the lowest energy singlet state in porphyrins is labeled Q_x, whereas the lowest energy singlet state in chlorins is labeled Q_y.

The classic porphyrin sensitizers used in PDT, such as protoporphyrin IX and Photofrin, are characterized by low two-photon cross sections.[37,38] This led to the development of porphyrinoids with enhanced nonlinear optical properties. These structures include, *inter alia*, diporphyrins,[39,40] asymmetric *meso*-substituted molecules[41−44] and π-expanded macrocycles,[45−47] polymer-templated *J*-aggregates,[48] and self-assembled supramolecular porphyrin chains.[49−52] The modified structures are still capable of generating $^1O_2$ via energy transfer processes, the mechanism of which is referred to as Type II PDT. Note that the Type I (electron transfer) and Type II (energy transfer) nomenclature associated with PDT are separate from the Type I and Type II two-photon processes described in detail below.

In this study, we examine the two-photon properties of the low-lying Q-bands of porphyrin and chlorin derivatives. The majority of previous studies have been directed at the Soret bands, which have intrinsically large oscillator strengths. When substituents are added that induce charge transfer character into the Soret band, the Soret bands have been shown to gain high two-photon absorptivities.[40,45,47,53,54]

We prepared a series of strongly fluorescing porphyrinoids that allow a systematic study of the effects of "single-point" modulations of the chromophore itself, also varying symmetry and dipole moments (Scheme 1). The parent compound, *meso*-tetraphenyl-porphyrin (**TPP**), was converted, in three steps, to the stable symmetric chlorin, *meso*-tetraphenyl-2,3-dimethoxy-chlorin [(**OMe**)$_2$**TPC**].[55] A two-step oxidation of **TPP** replaced a porphyrin double-bond with a lactone moiety, generating *meso*-tetraphenyl-porpholactone (**TPL**).[56] From previous studies, we knew that this compound showed some spectral characteristics of a porphyrin and a chlorin.[56] Lastly, a reduction of the lactone generated *meso*-tetraphenyl-porpholactol [(**OH**)**TPO**], a typical chlorin but with an asymmetric chromophore.[56] We have shown previously that the replacement of an sp^3-carbon by an oxygen led to enhanced single-photon absorptivities.[56] In addition, a comparison of porphyrin

Scheme 1. Structures and Synthetic Pathways of the β,β'-Modified Chromophores Investigated

meso-tetraphenyl-porphyrin, **TPP**

1. OsO₄, py
2. H₂S

meso-tetraphenyl-2,3-dihydroxychlorin

MeI, NaH

meso-tetraphenyl-2,3-dimethoxychlorin **(OMe)₂TPC**

MnO₄⁻

meso-tetraphenylporpholactone (*meso*-tetraphenyl-2-oxa-3-oxoporphyrin) **TPL**

1. Zn(acetate)₂
2. DIBAL-H
3. H⁺

meso-tetraphenylporpholactol (*meso*-tetraphenyl-2-oxa-3-hydroxychlorin) **(OH)TPO**
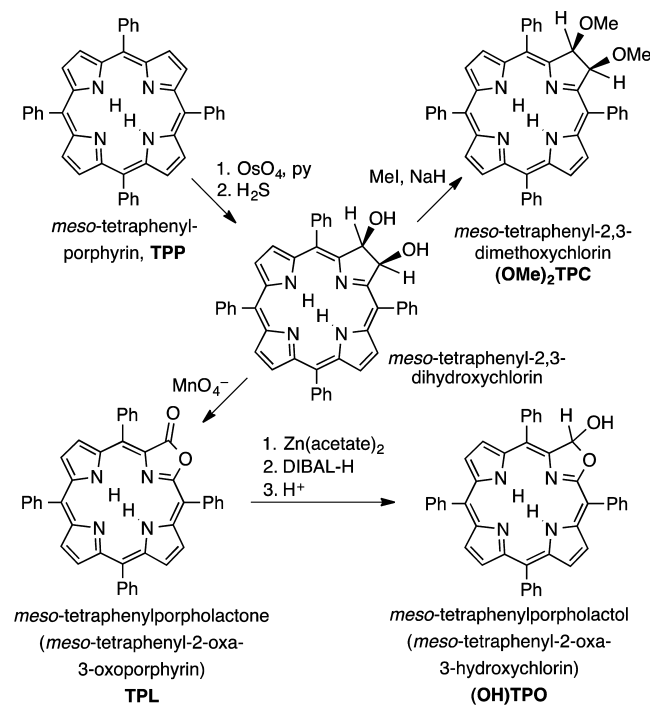
with **TPP** allows the study of the influence of the presence of *meso*-phenyl groups.

The primary goal of this study is to understand both the vibronic and electronic characteristics responsible for the nonlinear optical properties of the Q-bands in porphyrins and chlorins. The principal value of this series of molecules is the opportunity to more fully characterize the mechanism of two-photon absorption into excited states in cases where absorptivity was not gained through resonance with lower-lying states. We will also demonstrate that despite the low one-photon oscillator strengths of the Q-bands, large two-photon absorptivities are possible when the chromophore is derivatized in a way that introduces some degree of chromophore nonplanarity.

■ EXPERIMENTAL SECTION

Materials. Porphin was purchased from Frontier Scientific (Logan, UT) and rhodamine 6G and rhodamine B were purchased from Eastman Kodak Company (Rochester, NY). All other chromophores were prepared as described in the literature: **TPP** was synthesized according to the method of Adler;[57] **(OMe)₂TPC** was prepared by dihydroxylation of **TPP** and subsequent alkylation of the intermediate dihydroxychlorin;[55] oxidation of the intermediate dihydroxychlorin generated **TPL**;[56] reduction of the lactone generated the oxazolochlorin, **(OH)TPO**.[56] Solvents were spectroscopic grade (Aldrich) and were used as received.

Sample Preparation. For both one-photon and two-photon spectroscopy, the porphyrinoids were dissolved in carbon disulfide (CS₂). Carbon disulfide was chosen as a solvent environment for four reasons: (1) it has a high refractive index (η = 1.628), (2) it is a reasonable solvent for the compounds investigated in terms of solubility, (3) there is no major solvent absorption band in the visible and NIR regions of interest, and (4) the lack of absorbing vibrational

modes also avoids the thermal shock events that limit the repetition rate of two-photon excitation studies and that add an additional source of noise to the experiments. The sample solutions were placed in a 1 × 1 cm² glass cuvette to minimize secondary harmonic generation, which is known to reduce two-photon induced events. The sample optical density (OD) was adjusted to be 1−1.5 for linear measurements and 6−10 for nonlinear measurements.

Rhodamine 6G and rhodamine B, dissolved in ethanol, methanol, and 95:5 CS₂:methanol (v/v), were used as standards for the fluorescence quantum efficiency and two-photon absorptivity measurements. Because rhodamine 6G and rhodamine B are insoluble in CS₂, 5% methanol was added to solvate the compounds, and a minimal volume of hexafluoroisopropanol (HFIP) was added as a deaggregating agent.

Two-Photon Absorption Spectroscopy. The two-photon excitation spectra were collected by using the tunable pulsed-laser spectrometer shown in Figure 3. The spectroscopic
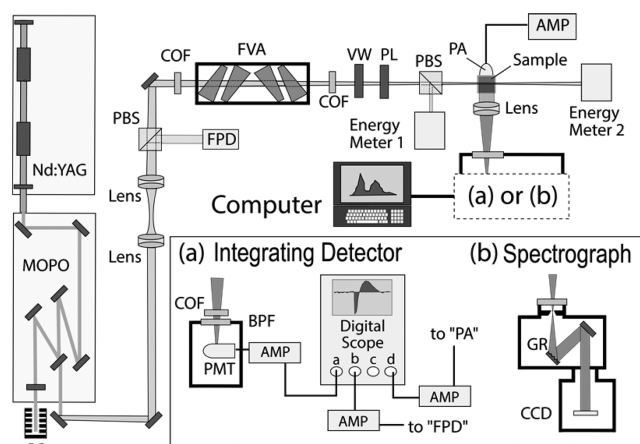
Figure 3. Schematic of the two-photon spectroscopy system used to obtain the nonlinear optical spectra reported here.[58] The system can simultaneously observe two-photon induced fluorescence and photoacoustic signals, but all the data reported here are based on fluorescence excitation, which provided a better signal-to-noise ratio. Abbreviations: AMP (amplifier), BPF (band-pass filter), BS (beam stop), COF (cutoff filter), FPD (fast photodiode), FVA (Fresnel variable attenuator), GR (grating), PA (photoacoustic detector), PBS (pellicle beam splitter), PL (polarizer), PMT (photomultiplier tube), VW (variable waveplate).

methods were identical to those used by us previously.[58] The two-photon spectrum was scanned for each molecule from 800 to 1400 nm and the two-photon character of the process was verified by fitting the magnitude of the fluorescence signal versus the intensity of the excitation beam. Sample results are shown in Supporting Information Figure S2, and the details are explored below.

We now examine the extent to which the spectra we report here can be verified as pure two-photon in origin. Data were collected for four molecules at various wavelengths, and we examine here the results for an analysis of **TPP** at 1200 nm. This study showed the highest multiphoton contamination, due primarily to the fact that **TPP** is not one of the stronger two-photon absorbers, and the wavelength of excitation intercepted a relatively weak two-photon vibronic feature (see Supporting Information Figure S4).

We used singular value decomposition (SVD) based regression to fit the signal versus laser intensity to equations of the form

$$\text{Signal} = a \times E_{\text{pulse}}^{i} + b \times E_{\text{pulse}}^{j} + \dots + d \times E_{\text{pulse}}^{l} \quad (1)$$

where a, b, $\cdots$, d are parameters fit by the SVD analysis for fixed values of the integers i, j, $\cdots$, l. The best fit equation was assigned by minimizing the product of the RMS error and the number of fit parameters. The best fit was found for $i = 2$ and $j = 3$ (see Supporting Information Figure S1)

$$\text{Signal} = 24.864 \times E(\text{mJ})^2 + 0.83575 \times E(\text{mJ})^3 \quad (2)$$

We use energy as the independent variable in these analyses because the energy is directly measured (Figure 3) and is linearly proportional to the intensity because the pulse width is constant. Equation 2 indicates that the observed signal has increasing three-photon character as the excitation energy increases, and reaches 5.7% at pulse energies of 1.8 mJ. We recognized this potential source of error early on in our studies, and limited the excitation energies used in all of our experiments to the range $0.6 \text{ mJ} \leq E_{\text{pulse}} \leq 1.1 \text{ mJ}$ to make sure that the two-photon component of the signal would be 96% or greater (see Supporting Information Figure S1). A potential outlier in this regard is porphin, which has Q_x and Q_y two-photon absorptivities even smaller than those of **TPP** (see below). However, a regression analysis at the two-photon maximum indicated no higher order components of the signal above that associated with noise.

Absolute two-photon absorptivities were measured by using rhodamine B in methanol or methanol/CS_2 as an external standard.[59] The excitation measurements followed the methods described in the literature.[15] The photoacoustic measurements used bacteriorhodopsin as an external standard.[60] The results agreed to within 12%, but the final results are reported based on the excitation measurements due to a larger signal-to-noise ratio. The absolute two-photon absorptivities are plotted in Supporting Information Figure S3 and tabulated in Supporting Information Table S1.

One-Photon Absorption Spectroscopy. All one-photon absorption spectra were measured using a Cary 50 UV−visible spectrophotometer. Oscillator strengths of the bands were determined by assigning the vibronic features to the Q_x or Q_y states as shown in Supporting Information Figures S4 and S5, and integrating the respective regions.

Fluorescence Quantum Yields. Rhodamine 6G and rhodamine B were used as standards, in which the fluorescence quantum yield (Φ_F) in ethanol is known to be 0.95 and 0.65, respectively.[59] The Φ_F values of the porphyrinoid samples were measured by using the following formula

$$\frac{\int I_{F,X}}{\int I_{F,ST}} = \frac{\Phi_{F,X}}{\Phi_{F,ST}} \left(\frac{\eta_X^2}{\eta_{ST}^2} \right) \quad (3)$$

where $\int I_{F,X}$ and $\int I_{F,ST}$ are the integrated fluorescence spectra, $\Phi_{F,X}$ and $\Phi_{F,ST}$ are the fluorescence quantum yields, and η_X and η_{ST} are the refractive indices of the solvents used for measurement, all with respect to unknown (X) and standard (ST) samples for the measurements, respectively.

Determination of Two-Photon Properties. The two-photon properties of the porphyrinoids investigated were calculated by using a variety of theoretical methods for comparison. All calculations were based on the orientationally averaged procedures originally proposed by Monson and McClain,[61] and as implemented by Masthay et al.[62] The equations can be simplified if both photons have the same energy, as is the case in the present study, in which a single laser is used to induce the two-photon event. The two-photon absorptivity at the two-photon absorption maximum (δ_{f0}) is given by

$$\delta_{f0} = \frac{(2\pi e)^4}{(4\pi\varepsilon_0 ch)^2} [E_\lambda^2 g_{\text{max}}(2E_\lambda)]|S_{f0}(\lambda, \lambda)|^2 \quad (4)$$

where E_λ is the energy of the photon, $g_{\text{max}}(2E_\lambda)$ is the maximum value of the normalized line shape function described below, and S_{f0} is given by

$$|S_{f0}(\lambda, \lambda)|^2 = \frac{1}{30} \sum_i^N \sum_j^N S_{ij}^{(f)} \quad (5)$$

and

$$S_{ij}^{(f)} \begin{cases} \dfrac{a(\langle i|\mathbf{r}|0\rangle \cdot \langle f|\mathbf{r}|i\rangle)(\langle j|\mathbf{r}|0\rangle \cdot \langle f|\mathbf{r}|j\rangle)}{[(E_i - E_\lambda)(E_j - E_\lambda)\Gamma^2]} + \\[2ex] \dfrac{b(\langle i|\mathbf{r}|0\rangle \cdot \langle j|\mathbf{r}|0\rangle)(\langle f|\mathbf{r}|i\rangle \cdot \langle f|\mathbf{r}|j\rangle)}{[(E_i - E_\lambda)(E_j - E_\lambda)\Gamma^2]} + \\[2ex] \dfrac{b(\langle i|\mathbf{r}|0\rangle \cdot \langle f|\mathbf{r}|j\rangle)(\langle f|\mathbf{r}|i\rangle \cdot \langle j|\mathbf{r}|0\rangle)}{[(E_i - E_\lambda)(E_j - E_\lambda) + \Gamma^2]} \end{cases} \quad (6)$$

Note that the sum over states in eq 5 includes the initial and final states.[62−64] The variables a and b in eq 6 specify the polarization of the two photons. For two photons propagating along the same path with identical polarization, a and b both equal 8. Other polarization and propagation situations are given in Table 1 of ref 62. A damping constant of $\Gamma = 2$ eV was used to prevent fortuitous resonances from "blowing up". The function $g_{\text{max}}(2E_\lambda)$ has units of seconds and is normally approximated by using a Gaussian distribution.[62] That approach, however, is not adequate for the present investigation. The Q-bands of porphyrins and chlorins display discrete vibronic structure with two or more separate vibronic bands. In such cases, the line shape function must be assigned for each final state by integrating under the normalized two-photon spectrum in frequency space and setting g_{max} equal to the inverse of the integral

$$g_{\text{max}} = \left[\int_0^\infty \hat{\delta}(\nu)\, d\nu \right]^{-1} \quad (7)$$

where $\hat{\delta}(\nu)$ is the normalized and dimensionless function that represents the two-photon spectrum in frequency space. There is some confusion in the literature regarding this function.[15] It is not the integral that is normalized, but rather the function, so that $\hat{\delta}(\nu_{\text{max}}) = 1$, where ν_{max} is the frequency of maximum two-photon absorption.

The key difficulty in calculating the two-photon absorptivity is the necessity to generate the many transition energies, transition lengths, and dipole moments that appear in the summation of states (SOS) in eq 6. We used both semiempirical MNDO-PSDCI procedures[58,65,66] and a hybrid *ab initio* approach using both the symmetry-adapted cluster-configuration interaction (SAC−CI)[67−70] and full single configuration interaction (CIS)[71] methods. The semiempirical MNDO-PSDCI method used calculates excited state properties

Table 1. One-Photon and Two-Photon Properties of the Lowest Two Excited Singlet States of Selected Porphyrins and Chlorins[a]

Property[b]	Porphin	TPP	(OH) TPO	(OMe)$_2$TPC	TPL
One-Photon (obsvd)					
ΔE (S$_1$ state, 0,0) /eV	1.998	1.894	1.899	1.909	1.919
ΔE (S$_1$ state, max) /eV	2.182	2.083	2.068	2.073	2.088
f (S$_1$ state)	0.0388	0.0378	0.0849	0.0447	0.0463
ΔE (S$_2$ state, 0,0) /eV	2.500	2.237	2.227	2.252	2.202
ΔE (S$_2$ state, max) /eV	2.500	2.385	2.380	2.376	2.361
f (S$_2$ state)	0.0177	0.0135	0.1171	0.0847	0.1224
Fluorescence Q Yield	0.05	0.09	0.39	0.26	0.07
Figures	4 and S4	4 and S4	4 and S5	4 and S5	4 and S5
One-Photon (calcd)					
ΔE (S$_1$ state) /eV	1.9787	2.1075	2.1244	2.1065	2.1505
f (S$_1$ state)	0.0020	0.0079	0.0796	0.0419	0.0078
ΔE (S$_2$ state) /eV	2.5583	2.8387	2.8520	2.9270	2.6903
f (S$_2$ state)	0.0009	0.0017	0.0681	0.0341	0.0728
Figure	7	7	8	8	8
Two-Photon (obsvd)					
ΔE (S$_1$ TPE max) /eV	2.192	2.080	2.078	2.078	2.098
g_{max} (S$_1$ state) /(s × 10^{-14})	4.543	3.867	3.161	3.892	3.949
δ (S$_1$ TPE max) /GM[b,c]	0.023	2.37	43.7	67.6	30.5
ΔE (S$_2$ TPE max) /eV	2.643	2.252	2.237	2.237	2.229
g_{max} (S$_2$ state) /(s × 10^{-14})	1.378	1.900	1.932	2.271	1.443
δ (S$_2$ TPE max) /GM[b,c]	0.022	1.15	37.6	54.9	6.8
Figures	4 and S6	4 and S6	4 and S7	4 and S7	4 and S7
Two-Photon (calcd):[d]					
1/2[δ(S$_1$) + δ(S$_2$)]/GM hybrid	0.0	0.14	83	54	23
1/2[δ(S$_1$) + δ(S$_2$)]/GM mndoci	0.0	0.86	25	22	18

[a]Ambient temperature in CS$_2$ unless noted otherwise. [b]Two-photon absorptivities are in Göppert-Mayers (GM) where 1 GM = 10^{-50} cm^4 s. [c]Observed absolute two-photon absorptivities are estimated to have an error of ±15% and use rhodamine as the external standard (Supporting Information Table S1, Figure S3). [d]Calculated by using the methods described in the text.

by implementing full single and double configuration interaction within the π system.[58,65,66] The code is available upon request from RRB. All MNDO-PSDCI calculations reported here used the standard parametrization, which assigns the σ and π mobility constants an identical value of 1.7, the Nishimoto-Mataga approximation for electron-repulsion integrals,[72] and the AM1[73] Hamiltonian.[58,65,66] The SOS calculations included the lowest 60 excited singlet states. The hybrid approach used the SAC−CI method to calculate the dipole moments in the ground and first two excited singlet states and the oscillator strengths into these states. The CIS method was used to assign the transition energies and transition lengths between the lowest 40 excited singlet states.

Ground-state geometries were calculated by using density functional theory (DFT) methods, the B3LYP functional, and the 6-31G(d) basis set.[74] The effect of solvent environment on both the ground-state geometries and transition energies was calculated by using the polarizable continuum model (PCM) method.[75−78] We observed that the calculated two-photon absorptivities were very sensitive to the ground-state geometry, and that the chlorin ring system was remarkably flexible. This resulted in greatly reduced rotational barriers for *meso*-phenyl groups. We also observed that ground-state geometries based on well-studied semiempirical Hamiltonians, such as MOPAC/PM3 and MOPAC/PM6, generated equilibrium geometries that included significant distortion from planarity in the ring system. Surprisingly, these geometries often generated two-photon absorptivities that were in much better agreement with the experiment than those generated by using the B3LYP/6-31G(d) DFT methods. Thus, we explored both DFT and semiempirical ground-state geometries.

■ RESULTS AND DISCUSSION

Experimental One-Photon and Two-Photon Spectra. The one-photon and two-photon spectra of the porphyrinoids studied in the Q-band region are shown in Figure 4. The vibronic features are assigned based on the oversimplified notion that there is a single promoting mode. This approach works reasonably well for the *meso*-tetraphenyl-substituted compounds, but is not adequate for unsubstituted porphin, which exhibits a much more complex vibronic development (Figure 4). A comparison of the one-photon and two-photon spectra indicates that the vibronic distributions of the linear and nonlinear spectra are different. For example, the 1,0-vibronic component of the lowest singlet state is the most intense feature in all of the two-photon spectra. In contrast, the one-photon spectra do not display a dominant vibronic mode, nor do the Q-bands display consistent relative intensities. One of the key goals of this paper is to provide an explanation for these vibronic anomalies.

One-Photon and Two-Photon Vibronic Distributions. We can calculate the vibronic distribution of a two-photon transition by replacing the $S_{f0}^{(\lambda\lambda)}$ in eq 4 with a Taylor's series with respect to the normal coordinate, Q_a.[79] The resulting expansion provides the two-photon absorptivity in terms of the individual vibrational modes, v'_k, within the final excited state manifold

$$S_{f0}^k = S_{f0}^e(Q_{eq})\langle v'_k|0''\rangle + \sum_a \frac{\partial S_{f0}^e}{\partial Q_a}\langle f|Q_a|0\rangle + \dots \quad (8)$$

The first term on the right-hand side of eq 8 assumes that the transition occurs from the zero vibrational level in the ground state and represents the first term of the Taylor expansion, where $S_{f0}^e(Q_{eq})$ is the pure electronic contribution evaluated at the ground-state equilibrium geometry (Q_{eq}) and is the Franck−Condon overlap integral between the vibrational mode in the final excited state and the zero point level in the ground state (0″). The second term on the right-hand side represents the contribution from second order effects, in which vibrational modes mediate the electronic transition probability, and will be ignored in our simulations. Substituting for $S_{f0}^{(\lambda\lambda)}$ in eq 4 and including the energy term, the vibronic distribution in the final state takes the form
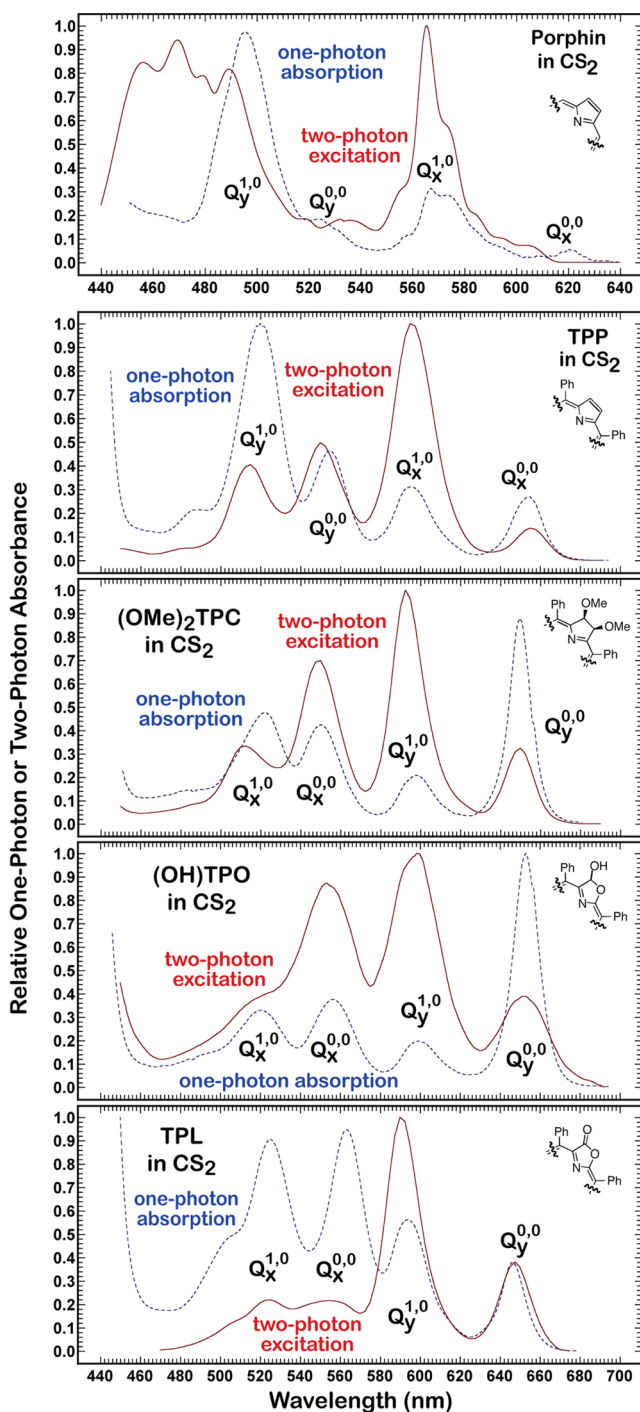
Figure 4. Ambient temperature one-photon absorption (dashed, blue trace) and two-photon excitation (red, solid trace) spectra of the porphyrinoids indicated in CS$_2$. The two-photon data are plotted relative to the wavelength of the final state transition associated with the simultaneous absorption of the two photons. The vibronic bands are marked using a simple notion that each electronic state contributes a system origin (0,0) and a higher energy vibronic component (1,0).

$$\delta_{f0}^{k} \propto P\left[\Gamma[\psi_{vib}^{k}] \otimes \Gamma[\psi_{elec}^{f}] \in \left\{\begin{array}{c}\xi^2 \\ xy \\ xz \\ yz\end{array}\right\}\right]\frac{E_{k0}^{f}}{E_{00}^{f}}|\langle v_k'|0''\rangle|^2 \quad (9)$$

where the symmetry function, P[...], returns unity when the product of the electronic and vibrational symmetries are two-photon allowed (and zero otherwise), and E_{k0}^{f} is the energy of the transition from the ground state to the kth mode in the final state. The Franck−Condon overlap integral, $\langle v_k'|0''\rangle$, is calculated by generating the vibrational modes in the ground state and in the final excited state and matching up the modes. Thus, each mode, k, has a potentially different frequency in the ground and excited state, and will likely be associated with a different effective reduced mass. Provided the polyatomic molecule has high symmetry so that the vibrational modes are divided up into symmetry groups, matching the modes is a straightforward process. The principal variable in assigning the Franck−Condon distribution for a given mode is the displacement upon excitation, or simply Δ_k. We used *Gaussian 09* and the method proposed by Niedzwiedzki et al.[80] to calculate this dimensionless displacement for the kth mode

$$\Delta Q_k^{f0} = \Delta_k = 95.76 \left\|\left[\frac{1}{(\mu_j)^{1/3}(\sigma_j)^{2/3}} - \frac{1}{(\mu_i)^{1/3}(\sigma_i)^{2/3}}\right]\right\|_k \quad (10)$$

where σ_i is the frequency and μ_i is the reduced mass of the kth mode in the ground state, and σ_j and μ_j are the corresponding values for the kth mode in the excited state. The prefactor assumes that the frequencies are in wavenumbers (cm^{-1}) and the reduced masses are in amu. The key advantage of eq 10 is the partial compensation for the Duschinsky effect, which is reflected in a change in the reduced mass of the mode upon excitation.

What remains is to calculate the Franck−Condon vibrational overlap integrals. The calculation is facilitated by using the very efficient, closed form expansions proposed by Chang for displaced and distorted harmonic oscillators.[81] We carried out the calculations for porphin and the corresponding chlorin (2,3-dihydroporphin) molecule for which the vibrational mode assignments are unambiguous. The Franck−Condon active vibrational modes are listed in Supporting Information Tables S2 and S3, and the resulting vibronic distributions are shown in Figure 5. Note, however, that some of these modes are active in the one-photon spectra, whereas others are active only in the two-photon spectra, as determined by evaluation of the function P[...] in eq 9.

Despite the significant approximations inherent in the results shown in Figure 5, these simulations provide an excellent perspective on why the one-photon and two-photon vibronic distributions are different. First, the system origin is relatively weak in the two-photon spectra because all of the electronic states studied here are two-photon forbidden. Two-photon bands appearing in the region of the system origin are due to low-frequency modes, or hot bands, which were not included in these simulations. Second, the most intense band in the two-photon spectra is the second vibronic band, which is made up of a significant number of vibronic bands that are unique to the two-photon vibrational manifold. In contrast, the one-photon spectra involve many fewer contributing promoting modes.

Two-Photon Absorptivities. Molecules absorb two photons via two possible mechanisms, as schematically shown in Figure 6 based on semiclassical single intermediate state two-photon theory.[16] Two-photon absorption events can be viewed as a two-step process, even though these two events typically happen within less than 1 fs. The first photon interacts with the
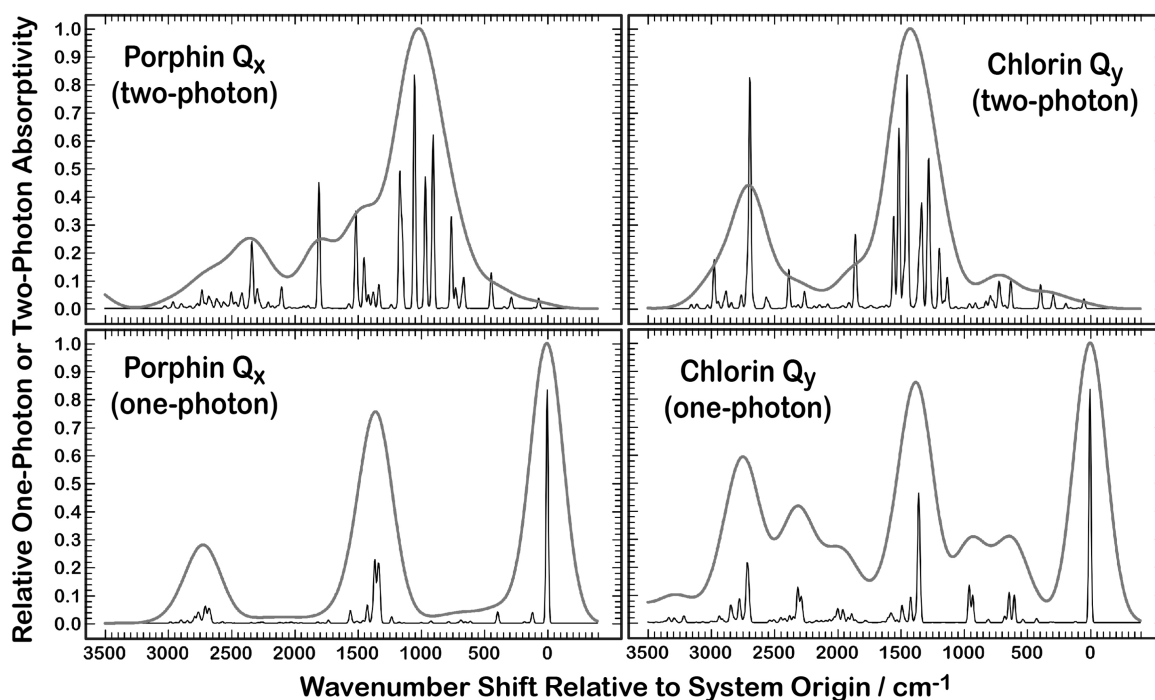
Figure 5. Simulations of the vibronic band development in the lowest lying Q-bands of the porphin Q_x band (left) and chlorin (2,3-dihydroporphin) Q_y band (right) under one-photon (lower) and two-photon (upper) selection rules.
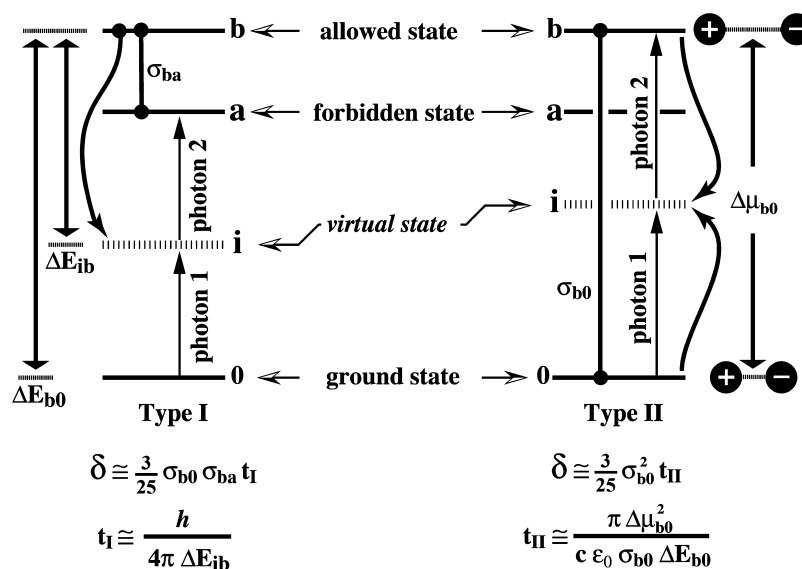
Figure 6. Two principal mechanisms of two-photon absorption are compared based on semiclassical two-photon theory.[16,58] The Type I process (left) is important for excited states which are one-photon forbidden. A strongly allowed one-photon state can also be a two-photon allowed state via a Type II process (right) if it undergoes a change in dipole moment upon excitation ($\Delta\mu$). The equations shown are based on a single intermediate state approximation and assume further that both photons have parallel polarization and propagation, and equal energy. The σ_{ij} variables are one-photon cross sections and are in units of length squared. The t_I and t_{II} equations calculate the expectation value of the lifetime of the virtual state, i. These equations are for vacuum conditions, where ε_0 is the vacuum permittivity.

molecule and prepares what is known as a virtual state (i). The virtual state is not a stationary state of the molecule, but is created momentarily during the forward scattering of the first photon.

In the Type I process, the stationary state is mediated by a nearby strongly allowed state, which exhibits large one-photon cross sections between the final state (σ_{ba}) and the ground state (σ_{b0}). If we assume the allowed state is separated from the virtual state by 1.5 eV, then the lifetime of the virtual state, t_I, is

~0.22 fs. If we assume a strong one-photon cross section of σ_{b0} = σ_{ba} = 10^{-16} cm^2, then the Type I process has a two-photon absorptivity of 26 × 10^{-50} cm^4 s (26 GM).

Calculation of the corresponding lifetime for a Type II process is more complicated, as this process depends on the photophysical properties of both the initial and final states. If the transition is strongly allowed and the dipole moment changes upon excitation, a Type II process can lead to very large two-photon absorptivities. Let us assume the transition

Porphin in CS$_2$	TPP (vacuum)	TPP in CS$_2$
Soret (B1U) State (16.3% dbls) μ= 0.0000 D ∂μ= 0.0000 D S$_3$ ∂E= 3.7016 eV f = 1.8356	Soret (AU) State (17.4% dbls) μ= 0.0000 D ∂μ= 0.0000 D S$_3$ ∂E= 3.9264 eV f = 2.3447	Soret (A) State (17.6% dbls) μ= 0.1367 D ∂μ= 0.0988 D S$_3$ ∂E= 3.9256 eV f = 2.1323
Qy (B2U) State (12.1% dbls) μ= 0.0000 D ∂μ= 0.0000 D S$_2$ ∂E= 2.5583 eV f = 0.0009	Qy (AU) State (11.9% dbls) μ= 0.0000 D ∂μ= 0.0000 D S$_2$ ∂E= 2.8500 eV f = 0.0054	Qy (A) State (11.5% dbls) μ= 0.0801 D ∂μ= 0.0630 D S$_2$ ∂E= 2.8387 eV f = 0.0017
Qx (B1U) State (14.2% dbls) μ= 0.0000 D ∂μ= 0.0000 D S$_1$ ∂E= 1.9787 eV f = 0.0020	Qx (AU) State (14.0% dbls) μ= 0.0000 D ∂μ= 0.0000 D S$_1$ ∂E= 2.1004 eV f = 0.0066	Qx (A) State (13.8% dbls) μ= 0.0516 D ∂μ= -0.0391 D S$_1$ ∂E= 2.1075 eV f = 0.0079
SAC-CI Calculation μ= 0.0000 D S$_0$ nsgl=806 ndbl=78925	SAC-CI Calculation μ= 0.0000 D S$_0$ nsgl=2050 ndbl=34403	SAC-CI Calculation CS2 μ= 0.0687 D S$_0$ nsgl=4096 ndbl=31594

Figure 7. SAC−CI analyses of the ground and low-lying excited singlet states (in vacuum and CS$_2$) of the porphyrins indicated. All calculations were carried out using an active space of 64 filled and 64 virtual orbitals. Solvent effects were approximated by using PCM methods. The charge distribution in the ground state is visualized by using blue to indicate regions of excess negative charge and red to indicate regions of excess positive charge. The shift in charge upon excitation is shown using contour lines, with red lines indicating excess positive charge and blue lines indicating excess negative charge. The arrows show the direction of the dipole moments.

occurs at ΔE_{b0} = 3 eV, has a strong one-photon cross-section of 10^{-16} cm^2, and exhibits a large change in dipole moment ($\Delta \mu$ = 10 D). The resulting virtual state lifetime is calculated to be 0.27 fs. Assuming $\sigma_{b0} = 10^{-16}$ cm^2 (see above), the Type II process has a two-photon absorptivity of δ_{II} = 33 GM, slightly larger than the Type I process (δ_I = 26 GM). Thus, there are two key molecular properties that make a Type II process important: a large change in dipole moment upon excitation and a final state that is strongly one-photon allowed. We note that the change in dipole moment, $\Delta \mu_{b0}$, is not the difference of the magnitude of the ground (0) and excited (b) state dipole moments, but represents the vectorial change as given below:

$$|\Delta \mu_{b0}| = [(\mu_b^{(x)} - \mu_0^{(x)})^2 + (\mu_b^{(y)} - \mu_0^{(y)})^2 + (\mu_b^{(z)} - \mu_0^{(z)})^2]^{1/2} \quad (11)$$

The low-lying Q-bands of the porphyrins or chlorins studied here do not correspond to strongly one-photon allowed transitions and no large changes in dipole moment upon excitation occur. The largest change in dipole moment calculated for any of the Q-bands studied here is less than 1 Debye. We can thus conclude that Type I processes will dominate for the molecules studied here. This prediction is confirmed by the detailed calculations reported below.

The properties of the low-lying excited singlet states under different solvent conditions based on SAC−CI molecular orbital theory are presented in Figures 7 and 8. The ground-state equilibrium geometry was assumed for all calculations, and hence the results are appropriate for Franck−Condon vertical excitations. The calculated two-photon absorptivities that are presented in Table 1 are based on the B3LYP/6-31G(d) equilibrium geometries and, in the case of the hybrid *ab initio* calculations, PCM-based solvent effects.

Calculations based on the equilibrium geometries predict that the second excited Q-band is the more two-photon allowed. In contrast, the experimental results indicate that the two Q-bands have comparable two-photon absorptivity with the exception of **TPL**, which has a second excited Q$_x$ absorptivity four times larger than that of the lower Q$_y$ band. We observed that the calculated two-photon absorptivities are extremely sensitive to conformation, and that while the relative two-photon absorptivities vary dramatically with conformation, the average of the Q$_x$ and Q$_y$ two-photon absorptivities are not overly sensitive to conformation. Hence, we reported the calculated averages in Table 1, and explore the fundamental issue in more detail below.

The first molecular variable we explored was the extent to which the phenyl groups influence the two-photon absorptivities. Porphin is the only molecule we studied without phenyl groups, and it is predicted to have no two-photon absorptivity in the ground resting state. However, if we populate individual vibrations in the ground state, we do calculate observable absorptivities (shown in Supporting Information Table S2 for porphin and Table S3 for chlorin). Hot bands impact the two-photon absorptivity via two mechanisms. The most important
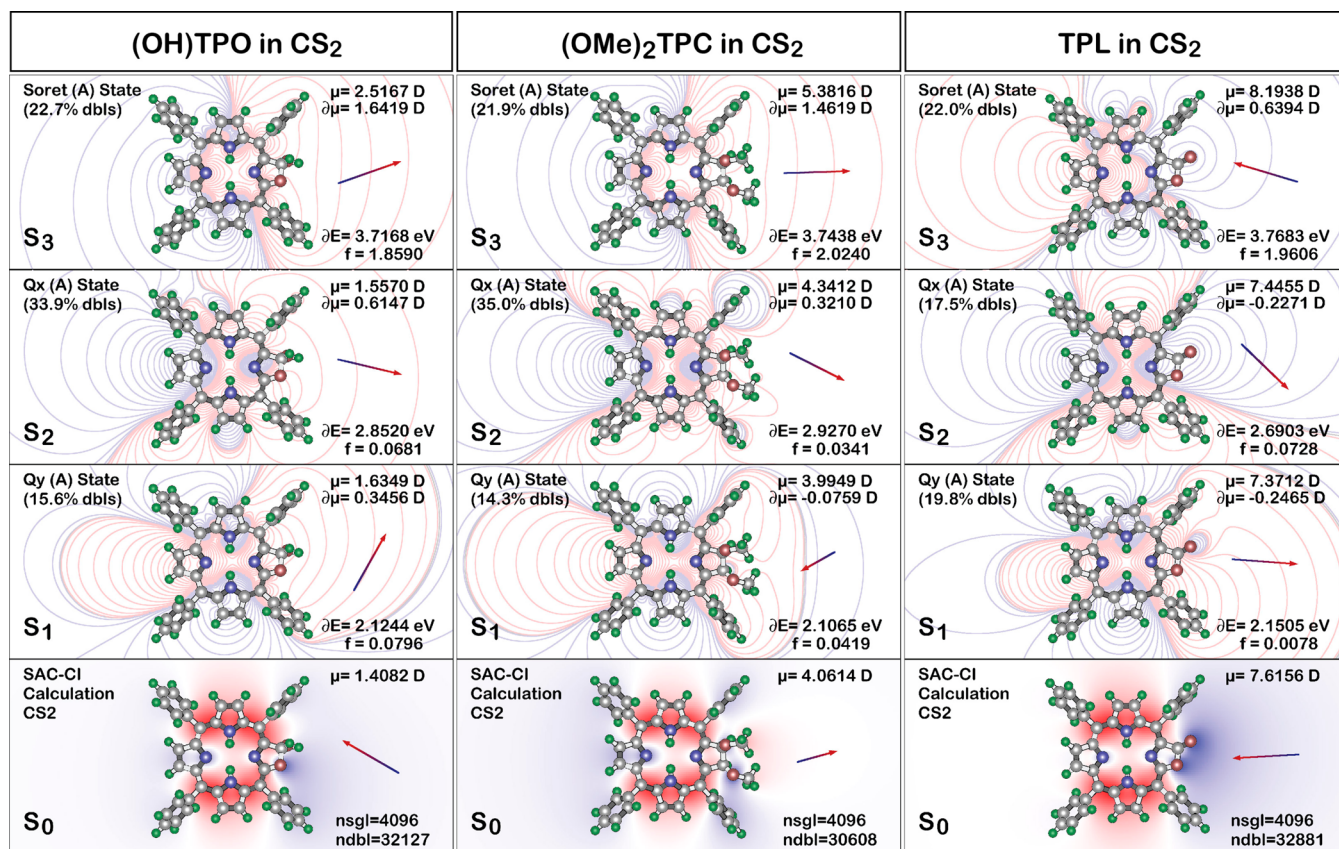
Figure 8. SAC−CI analyses of the ground and low-lying excited singlet states of the substituted chlorin-like porphyrinoids studied in this paper. Calculation details, contour plots, charge shifts upon excitation, and dipole moments are as described in Figure 7.

effect is the changing of the symmetry of the initial vibronic state, which is crucial, since in the absence of symmetry lowering, two-photon transitions into both Q_x and Q_y are symmetry forbidden. The second effect is to induce mixing of the singlet states by out-of-plane ring distortions. As the ring system forms a saddle-like conformation, the low-lying singlet states are mixed, and the Type I two-photon process is enhanced by increasing the magnitude of the transition lengths between the states. This process will be explored in more detail below as we examine why $(OMe)_2TPC$ has an anomalously high two-photon absorptivity.

Introduction of the phenyl groups to porphyrin has a number of effects. Partial rotation of the phenyl groups allows cross-talk between the phenyl- and the porphyrin-π systems, inducing mixing via conjugative interactions. In addition, the smaller the dihedral angle between the two planar systems, the larger the sterically induced ring out-of-plane distortions. The phenyl groups are observed to have a more important impact on the chlorins because the ring systems of the chlorins are more flexible,[82−84] allowing for a much reduced rotational barrier for phenyl group rotation at ambient temperature, thus allowing for a larger phenyl−chlorin interaction. The geometry of **TPP** in vacuum is C_i, but in solvent, the dispersive environment encourages the formation of a small dipole moment, which provides dipole-induced electrostatic stabilization.

The average experimental two-photon absorptivities of the two Q-bands increase in the following order: porphin < **TPP** < **TPL** < **(OH)TPO** < **(OMe)₂TPC**. In contrast, the calculated ordering is porphin < **TPP** < **TPL** < **(OMe)₂TPC** < **(OH)TPO**. The semiempirical and the *ab initio* (hybrid)

theoretical methods agree with each other on the ordering, and **(OMe)₂TPC** is the outlier when the results are compared with experiment. This compound is observed to have roughly twice the two-photon absorptivity as predicted (Table 1). The origin of this difference should provide fundamental insight into the mechanism of two-photon absorption in these molecules.

In the course of studying **(OMe)₂TPC**, we observed significant differences in the results based on how we calculated the ground-state geometry. Two different scenarios and their impact on the calculated two-photon properties are explored in Figure 9 and Table 2. When DFT methods [B3LYP/6-31G(d)] are used, **(OMe)₂TPC** is calculated to have a nearly planar ring structure (Figure 9A1 and A2) and the Q_x (S_2) state is calculated to have a majority of the two-photon absorptivity (Figure 9A, Table 2). In contrast, when semiempirical methods are used (MNDO/PM3), the geometry optimization yields a saddled geometry as shown in Figure 9B1 and B2. Supporting Information Table S4 presents a normal-coordinate structure decomposition (NSD) of the **(OMe)₂TPC** structures depicted in Figure 9. The NSD procedure provides a numerical and qualitative description of the distortion of porphyrinoids in terms of displacement from a D_{4h} symmetric reference structure.[85,86] While the DFT structure of **(OMe)₂TPC** demonstrates modest saddling (B_{2u} mode) and ruffling (B_{1u} mode) distortions, the semiempirical structure exhibits a significant saddling (B_{2u} mode) distortion that is necessary to replicate the observed two-photon absorptivity. This ring distortion mixes the states and inverts the absorptivities such that the first excited singlet state has the highest two-photon absorptivity (Figure 9B, Table 2). This was the only molecule
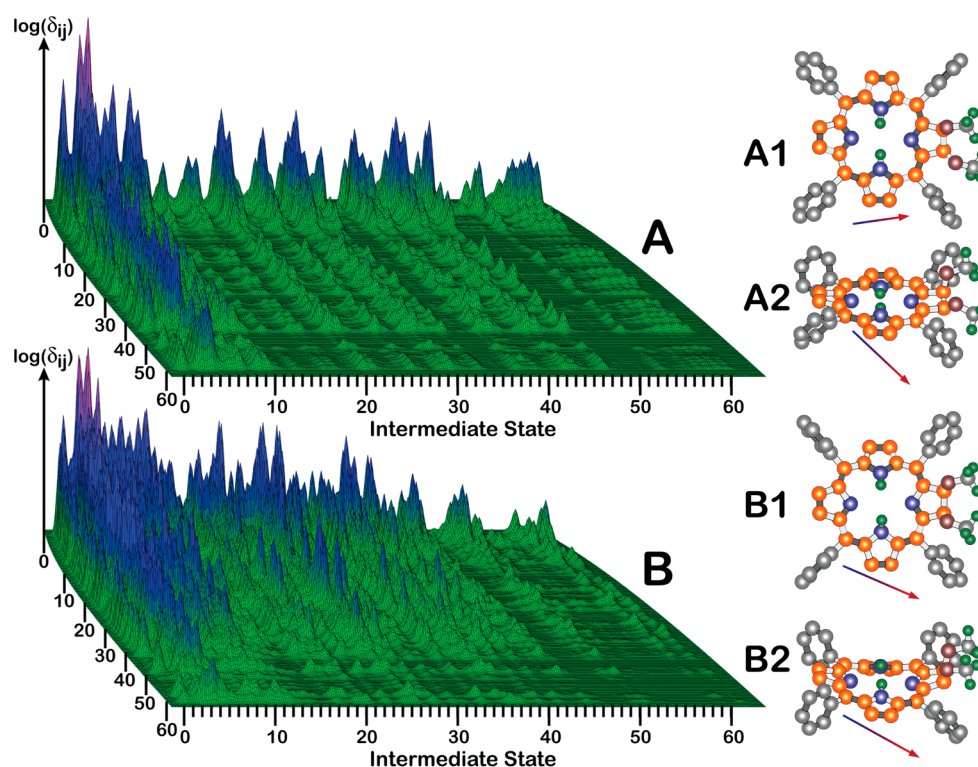
Figure 9. Analysis of intermediate state contributions to the calculated two-photon absorptivity of the Q_y band of $(OMe)_2TPC$ based on MNDO-PSDCI theory and 60 intermediate states. The height of each element is proportional to the log of the contribution of the matrix element to the two-photon absorptivity. The matrix shown in A is for the equilibrium geometry (A1, A2) as determined by DFT [B3LYP/6-31G(d)] for the molecule in CS_2 (PCM methods). The matrix shown in B is for a saddled ring conformation (B1, B2) generated by using MNDO/PM3 semiempirical methods.

for which PM3 geometries produced better agreement with experiment. The result does provide a perspective on the origin of the large two-photon absorptivity of $(OMe)_2TPC$ compared to the other systems studied: an on-average saddled ground-state conformation causes the Q_y and Q_x states to mix with higher excited states and thus lead to an enhanced two-photon absorptivity of both. This is visually expressed in Figure 9 (comparison of matrices A and B) by enhancement of the off-diagonal transition lengths creating additional contributions to the sum over states. In fact, the known solid state structures of porphin, **TPP**, **TPL**, $(OMe)_2TPC$, and $(OH)TPO$ also indicate that all are approximately planar but that $(OMe)_2TPC$ shows the largest distortions from ideality, in part due to the system trying to avoid an eclipsed conformation of the two methoxy groups on the pyrroline.

■ CONCLUSIONS

The simple planar porphyrins investigated here, including porphin and **TPP**, possess low-intensity Type I two-photon absorption processes in the Q-band region (0.02 and 2.37, respectively). The *meso*-phenyl groups do not contribute in a significant way to macrocycle distortion for **TPP**, which minimizes the enhancement of two-photon absorptivity. Porpholactone, **TPL**, also shows an anomalously small, porphyrin-like two-photon absorptivity maximum of 6.8 GM in the first excited (Q_y) singlet state. Both theory and experiment support a model of **TPL** with a nearly planar ground-state geometry. The vibronic development in the two-photon spectra of the chlorins $(OH)TPO$ and $(OMe)_2TPC$ is also significantly different from that observed in the one-photon spectra, with the $Q_y^{(1,0)}$ band exhibiting anomalous two-photon

intensity. Franck−Condon analyses indicated that both vibrational symmetry, which makes the system origin band weak, and Duschinsky-mediated mode displacements combine to enhance the higher (1,0) mode. Moreover, it was found that Type II processes contribute to the two-photon cross section of $(OH)TPO$ and **TPL**, but for no compound or geometry did we calculate a Type II contribution greater than 8% to the total absorptivity. Even though the single-photon absorption spectra of the chlorins $(OH)TPO$ and $(OMe)_2TPC$ are very similar, their two-photon absorptivities differ greatly. Chlorin $(OMe)_2TPC$ exhibits an anomalously large two-photon absorptivity maxima of 67.6 GM (Q_y) and 54.9 GM (Q_x), whereas the corresponding values for $(OH)TPO$ are 43.7 and 37.6. We attributed the high absorptivity of $(OMe)_2TPC$ to state mixing associated with a saddle ring conformation. Calculations on the static structures of the chlorin invariably predict that one of the Q-bands has much higher two-photon absorptivity than the other, but the experimental observation indicates that both bands have similar two-photon absorptivities. Calculations of the two-photon spectra indicated that the relative Q-band absorptivities are sensitive to the phase and magnitude of the chlorin ring distortions. The observation of comparable two-photon absorptivities indicated that the nonplanar conformations of $(OMe)_2TPC$ are in dynamic fluctuation in response to rapid torsional rotation of the phenyl groups. The high two-photon absorptivity in the 1000−1400 nm region is particularly advantageous for the potential utility of $(OMe)_2TPC$ in two-photon induced biomedical applications as the regime under ∼1100 nm falls within the optical window of biological tissue[87] and allows the use of solid-state Nd:YAG lasers (emission at 1064 nm). This work also points at saddled chlorin macrocycle conformations that should be incorporated

Table 2. Calculated Two-Photon Absorptivities for Selected Systems^{a,b}

geometry (method)	state	ΔE (eV)	$\langle A \rangle^b$	$\langle B \rangle^c$	$\langle C \rangle^d$	$\langle D \rangle^e$	$\langle C \rangle^d/\langle A \rangle^b$
			Porphin				
S$_0$ equilibrium	Q$_x$ (S$_1$)	2.5457	0.0	0.0	0.0	0.0	0.0
S$_0$ equilibrium	Q$_y$ (S$_2$)	2.6821	0.0	0.0	0.0	0.0	0.0
60 cm^{-1} (b3u) mode	Q$_x$ (S$_1$)	2.5316	0.1498	0.1124	0.2248	0.0375	1.5
60 cm^{-1} (b3u) mode	Q$_y$ (S$_2$)	2.6680	0.0348	0.0261	0.0521	0.0087	1.5
76 cm^{-1} (au) mode	Q$_x$ (S$_1$)	2.5200	0.1637	0.1228	0.2455	0.0419	1.5
76 cm^{-1} (au) mode	Q$_y$ (S$_2$)	2.6583	0.0349	0.0261	0.0523	0.0087	1.5
100 cm^{-1} (b3u) mode	Q$_x$ (S$_1$)	2.5355	0.0019	0.0015	0.0029	0.0005	1.5
100 cm^{-1} (b3u) mode	Q$_y$ (S$_2$)	2.6663	0.0034	0.0026	0.0052	0.0009	1.5
			Chlorin				
S$_0$ equilibrium	Q$_y$ (S$_1$)	2.4866	1.6164	1.2123	2.4246	0.4041	1.5
S$_0$ equilibrium	Q$_x$ (S$_2$)	3.1632	97.821	19.907	39.814	77.914	0.4070
37 cm^{-1} (a2) mode	Q$_y$ (S$_1$)	2.6518	3.4259	2.5694	5.1389	0.8565	1.5
37 cm^{-1} (a2) mode	Q$_x$ (S$_2$)	3.4797	155.55	27.15	54.29	123.40	0.3490
56 cm^{-1} (b1) mode	Q$_y$ (S$_1$)	2.6473	3.5149	2.6362	5.2723	0.8787	1.5
56 cm^{-1} (b1) mode	Q$_x$ (S$_2$)	3.4750	156.26	27.59	55.17	128.68	0.3531
92 cm^{-1} (a2) mode	Q$_y$ (S$_1$)	2.6397	3.3770	2.5328	5.0655	0.8443	1.5
92 cm^{-1} (a2) mode	Q$_x$ (S$_2$)	3.4689	156.25	27.49	54.98	128.76	0.3519
			Rhodamine B				
S$_0$ methanol (mndoci)	S$_1$	1.6255	168.07	56.59	113.18	111.48	0.6730
S$_0$ methanol (hybrid)	S$_1$	1.8208	34.360	27.753	51.504	8.6067	1.4990
			(OMe)$_2$TPC				
S$_0$ (PM3) (mndoci)	Q$_y$(S$_1$)	2.3525	105.90	36.40	72.81	69.49	0.6875
S$_0$ (PM3) (mndoci)	Q$_x$ (S$_2$)	2.5083	69.972	22.83	45.56	92.80	0.6526
S$_0$ CS$_2$ (hybrid)	Q$_y$(S$_1$)	2.4271	15.391	11.49	22.97	3.905	1.4925
S$_0$ CS$_2$ (hybrid)	Q$_x$ (S$_2$)	2.9810	106.97	26.13	52.26	80.84	0.4886

^{a}All two-photon absorptivities in Göppert-Mayers (10^{-50} cm^4 s). Vibrational hot band geometries were generated by using GaussView 5 based on a B3LYP/6-31G(d) force field calculation and a displacement level of unity. These geometries overestimate the displacement, and thus the enhanced two-photon absorptivity is overestimated as well. ^{b}Two-photon absorptivity calculated for both photons linearly polarized with parallel polarization. ^{c}Two-photon absorptivity calculated for both photons linearly polarized with perpendicular polarization. ^{d}Two-photon absorptivity calculated for both photons circularly polarized in the same sense with parallel propagation. ^{e}Two-photon absorptivity calculated for both photons circularly polarized in the opposite sense with parallel propagation.

into two-photon dyes designed for high absorptivity. We believe that the results of this study will prompt subsequent investigations that lead to optimized photosensitizers for clinical evaluations as NIR PDT photosensitizers.

ASSOCIATED CONTENT

Supporting Information

Two-photon absorptivities of the rhodamine B standard (Table S1), vibronic analyses of porphin and chlorin (Tables S2 and S3), normal-coordinate structure decomposition of **(OMe)$_2$TPC** (Table S4), regression analysis of the multi-photon excitation of **TPP** (Figure S1), fluorescence intensity vs incident excitation energy plot (Figure S2), two-photon excitation spectra of the rhodamine B standard (Figure S3), decomposition of the oscillator strengths of the Q$_x$ and Q$_y$ bands (Figures S4 and S5), and analyses of the maximum in the line shape functions, g_{max}, (Figures S6 and S7) for the porphyrinoids studied. This material is available free of charge via the Internet at http://pubs.acs.org.

AUTHOR INFORMATION

Corresponding Authors
*E-mail: c.bruckner@uconn.edu.
*E-mail: rbirge@uconn.edu.

Author Contributions
The manuscript was written through contributions of all authors. All authors have given approval to the final version of the manuscript.

ABBREVIATIONS

TPP, *meso*-tetraphenyl-porphyrin; **(OMe)$_2$TPC**, *meso*-tetraphenyl-2,3-dimethoxychlorin; **TPL**, *meso*-tetraphenyl-porpholactone; **(OH)TPO**, *meso*-tetraphenyl-porpholactol

REFERENCES

(1) Henderson, B. W.; Dougherty, T. J. How Does Photodynamic Therapy Work? *Photochem. Photobiol.* **1992**, *55*, 147−157.
(2) Drobizhev, M.; Sigel, C.; Rebane, A. Photo-Tautomer of Br-Porphyrin: A New Frequency-Selective Material for Ultrafast Time-Space Holographic Storage. *J. Lumin.* **2000**, *86*, 391−397.

(3) Rebane, A.; Kaarli, R.; Saari, P.; Anijalg, A.; Timpmann, K. Photochemical Time-Domain Holography of Weak Picosecond Pulses. *Opt. Commun.* **1983**, *47*, 173−176.

(4) Wood, G. L.; Miller, M. J.; Mott, A. G. Investigation of Tetrabenzoporphyrin by the Z-Scan Technique. *Opt. Lett.* **1995**, *20*, 973−975.

(5) Mathai, S.; Bird, D. K.; Stylli, S. S.; Smith, T. A.; Ghiggino, K. P. Two-Photon Absorption Cross-Sections and Time-Resolved Fluorescence Imaging Using Porphyrin Photosensitisers. *Photochem. Photobiol. Sci.* **2007**, *6*, 1019−1026.

(6) Finikova, O. S.; Lebedev, A. Y.; Aprelev, A.; Troxler, T.; Gao, F.; Garnacho, C.; Muro, S.; Hochstrasser, R. M.; Vinogradov, S. A. Oxygen Microscopy by Two-Photon-Excited Phosphorescence. *ChemPhysChem* **2008**, *9*, 1673−1679.

(7) Lecoq, J.; Parpaleix, A.; Roussakis, E.; Ducros, M.; Houssen, Y. G.; Vinogradov, S. A.; Charpak, S. Simultaneous Two-Photon Imaging of Oxygen and Blood Flow in Deep Cerebral Vessels. *Nat. Med.* **2011**, *17*, 893−898.

(8) Sakadžić, S.; Roussakis, E.; Yaseen, M. A.; Mandeville, E. T.; Srinivasan, V. J.; Arai, K.; Ruvinskaya, S.; Devor, A.; Lo, E. H.; Vinogradov, S. A.; et al. Two-Photon High-Resolution Measurement of Partial Pressure of Oxygen in Cerebral Vasculature and Tissue. *Nat. Methods* **2010**, *7*, 755−759.

(9) Spencer, J. A.; Ferraro, F.; Roussakis, E.; Klein, A.; Wu, J.; Runnels, J. M.; Zaher, W.; Mortensen, L. J.; Alt, C.; Turcotte, R.; et al. Direct Measurement of Local Oxygen Concentration in the Bone Marrow of Live Animals. *Nature* **2014**, *508*, 269−273.

(10) Collins, H.; Khurana, M.; Moriyama, E. H.; Mariapillai, A.; Dahlstedt, E.; Balaz, M.; Kuimova, M. K.; Drobizhev, M.; Yant, V. X. D.; Phillips, D.; et al. Blood-Vessel Closure Using Photosensitizers Engineered for Two-Photon Excitation. *Nat. Photonics* **2008**, *2*, 420−424.

(11) Wilson, B. C.; Patterson, M. S. The Physics of Photodynamic Therapy. *Phys. Med. Biol.* **1986**, *31*, 327−360.

(12) Sternberg, E. D.; Dolphin, D.; Brückner, C. Porphyrin-based Photosensitizers for Use in Photodynamic Therapy. *Tetrahedron* **1998**, *54*, 4151−4202.

(13) Muller, P. J.; Wilson, B. C. Photodynamic Therapy for Recurrent Supratentorial Gliomas. *Semin. Surg. Oncol.* **1995**, *11*, 345−354.

(14) Vrouenraets, M. B.; Visser, G. W. M.; Snow, G. B.; van Dongen, G. A. M. S. Basic Principles, Applications in Oncology and Improved Selectivity of Photodynamic Therapy. *Anticancer Res.* **2003**, *23*, 505−522.

(15) Birge, R. R. One-Photon and Two-Photon Excitation Spectroscopy. In *Ultrasensitive Laser Spectroscopy*; Kliger, D. S., Ed.; Academic Press, Inc.: New York, 1983; pp 109−174.

(16) Birge, R. R.; Pierce, B. M. Semi-Classical Time Dependent Theory of Two-Photon Spectroscopy. The Effect of Dephasing in the Virtual Level on the Two-Photon Excitation Spectrum of Isotachysterol. *Int. J. Quantum Chem.* **1986**, *29*, 639−656.

(17) Wan, S.; Parrish, J. A.; Anderson, R. R.; Madden, M. Transmittance of Nonionizing Radiation in Human Tissues. *Photochem. Photobiol.* **1981**, *24*, 679−681.

(18) Mroz, P.; Huang, Y.-Y.; Janjua, S.; Zhiyentayev, T.; Ruzie, C.; Borbas, K. E.; Fan, D.; Krayer, M.; Balasubramanian, T.; Yang, E. K.; et al. New Stable Synthetic Bacteriochlorins for Photodynamic Therapy of Melanoma. *Proc. SPIE* **2009**, *7380*, 73802S-1−73802S-14.

(19) Mroz, P.; Huang, Y.-Y.; Szokalska, A.; Zhiyentayev, T.; Janjua, S.; Nifli, A.-P.; Sherwood, M. E.; Ruzie, C.; Borbas, K. E.; Fan, D.; et al. Stable Synthetic Bacteriochlorins Overcome the Resistance of Melanoma to Photodynamic Therapy. *FASEB J.* **2010**, *24*, 3160−3170.

(20) Krayer, M.; Yang, E.; Kim, H.-J.; Kee, H. L.; Deans, R. M.; Sluder, C. E.; Diers, J. R.; Kirmaier, C.; Bocian, D. F.; Holten, D.; et al. Synthesis and Photophysical Characterization of Stable Indium Bacteriochlorins. *Inorg. Chem.* **2011**, *50*, 4607−4618.

(21) Krayer, M.; Yang, E.-K.; Diers, J. R.; Bocian, D. F.; Holten, D.; Lindsey, J. S. *De Novo* Synthesis and Photophysical Characterization of Annulated Bacteriochlorins: Mimicking and Extending the Properties of Bacteriochlorophylls. *New J. Chem.* **2011**, *35*, 587−601.

(22) Yang, E.; Diers, J. R.; Huang, Y.-Y.; Hamblin, M. R.; Lindsey, J. S.; Bocian, D. F.; Holten, D. Molecular Electronic Tuning of Photosensitizers to Enhance Photodynamic Therapy: Synthetic Dicyanobacteriochlorins as a Case Study. *Photochem. Photobiol.* **2012**, *89*, 605−618.

(23) Taniguchi, M.; Cramer, D. L.; Bhise, A. D.; Kee, H. L.; Bocian, D. F.; Holten, D.; Lindsey, J. S. Accessing the Near-Infrared Spectral Region with Stable, Synthetic, Wavelength-Tunable Bacteriochlorins. *New J. Chem.* **2008**, *32*, 947−958.

(24) Mroz, P.; Bhaumik, J.; Dogutan, D. K.; Aly, Z.; Kamal, Z.; Khalid, L.; Kee, H. L.; Bocian, D. F.; Holten, D.; Lindsey, J. S.; et al. Imidazole Metalloporphyrins as Photosensitizers for Photodynamic Therapy: Role of Molecular Charge, Central Metal and Hydroxyl Radical Production. *Cancer Lett.* **2009**, *282*, 63−76.

(25) Parusel, A. B. J.; Wondimagegn, T.; Ghosh, A. Do Nonplanar Porphyrins Have Red-Shifted Electronic Spectra? A DFT/SCI Study and Reinvestigation of a Recent Proposal. *J. Am. Chem. Soc.* **2000**, *122*, 6371−6374.

(26) Ryeng, H.; Ghosh, A. Do Nonplanar Distortions of Porphyrins Bring about Strongly Red-Shifted Electronic Spectra? Controversy, Consensus, New Developments, and Relevance to Chelatates. *J. Am. Chem. Soc.* **2002**, *124*, 8099−8103.

(27) Senge, M. O. Database of Tetrapyrrole Crystal Structure Determinations. In *The Porphyrin Handbook*; Kadish, K. M., Smith, K. M., Guilard, R., Eds.; Academic Press: San Diego, 2000; Vol. *10*, pp 1−218.

(28) Senge, M. O. Highly Substituted Porphyrins. In *The Porphyrin Handbook*; Kadish, K. M., Smith, K. M., Guilard, R., Eds.; Academic Press: Boston, 2000, Vol. *1*, pp 239−347.

(29) Gouterman, M. Spectra of Porphyrins. *J. Mol. Spectrosc.* **1961**, *6*, 138−163.

(30) Platt, J. R. Classification and Assignments of Ultraviolet Spectra of Conjugated Organic Molecules. *J. Opt. Soc. Am.* **1953**, *43*, 252−257.

(31) Brückner, C.; McCarthy, J. R.; Daniell, H. W.; Pendon, Z. D.; Ilagan, R. P.; Francis, T. M.; Ren, L.; Birge, R. R.; Frank, H. A. A Spectroscopic and Computational Study of the Singlet and Triplet Excited States of Synthetic β-Functionalized Chlorins. *Chem. Phys.* **2003**, *294*, 285−303.

(32) Hasegawa, J.; Ozeki, Y.; Ohkawa, K.; Hada, M.; Nakatsuji, H. Theoretical Study of the Excited States of Chlorin, Bacteriochlorin, Pheophytin *a*, and Chlorophyll *a* by the SAC/SAC−CI Method. *J. Phys. Chem. B* **1998**, *102*, 1320−1326.

(33) Flitsch, W. Hydrogenated Porphyrin Derivaties: Hydroporphyrins. *Adv. Heterocycl. Chem.* **1988**, *43*, 73−126.

(34) Whitlock, H. W.; Hanauer, R.; Oester, M. Y.; Bower, B. K. Diimide Reduction of Porphyrins. *J. Am. Chem. Soc.* **1969**, *91*, 7485−7489.

(35) Bonnett, R.; White, R. D.; Winfield, U. J.; Berenbaum, M. C. Hydroporphyrins of the *meso*-Tetra(hydroxyphenyl) porphyrin Series as Tumour Photosensitizers. *Biochem. J.* **1989**, *261*, 277−280.

(36) Gouterman, M. Study of the Effects of Substitution on the Absorption Spectra of Porphin. *J. Chem. Phys.* **1959**, *30*, 1139−1161.

(37) Goyan, R. L.; Cramb, D. T. Near-Infrared Two-Photon Excitation of Protoporphyrin IX: Photodynamics and Photoproduct Generation. *Photochem. Photobiol.* **2000**, *72*, 821−827.

(38) Karotki, A.; Khurana, M.; Lepock, J. R.; Wilson, B. C. Simultaneous Two-Photon Excitation of Photofrin in Relation to Photodynamic Therapy. *Photochem. Photobiol.* **2006**, *82*, 443−452.

(39) Kim, D. Y.; Ahn, T. K.; Kwon, J. H.; Kim, D.; Ikeue, T.; Aratani, N.; Osuka, A.; Shigeiwa, M.; Maeda, S. Large Two-Photon Absorption (TPA) Cross-Section of Directly Linked Fused Diporphyrins. *J. Phys. Chem. A* **2005**, *109*, 2996−2999.

(40) Drobizhev, M.; Stepanenko, Y.; Dzenis, Y.; Karotki, A.; Rebane, A.; Taylor, P. N.; Anderson, H. L. Extremely Strong Near-IR Two-Photon Absorption in Conjugated Porphyrin Dimers: Quantitative Description with Three-Essential-States Model. *J. Phys. Chem. B* **2005**, *109*, 7223−7236.

(41) Nowak-Król, A.; Wilson, C. J.; Drobizhev, M.; Kondratuk, D. V.; Rebane, A.; Anderson, H. L.; Gryko, D. T. Amplified Two-Photon Absorption in *Trans*-A₂B₂-Porphyrins Bearing Nitrophenylethynyl Substituents. *ChemPhysChem* **2012**, *13*, 3966−3972.

(42) Koszelewski, D.; Nowak-Król, A.; Drobizhev, M.; Wilson, C. J.; Haley, J. E.; Cooper, T. M.; Romiszewski, J.; Górecka, E.; Anderson, H. L.; Rebane, A.; et al. Synthesis and Linear and Nonlinear Optical Properties of Low-Melting π-Extended Porphyrins. *J. Mater. Chem. C* **2013**, *1*, 2044−2053.

(43) Karotki, A.; Kruk, M.; Drobizhev, M.; Rebane, A.; Nickel, E.; Spangler, C. W. Efficient Singlet Oxygen Generation Upon Two-Photon Excitation of New Porphyrin With Enhanced Nonlinear Absorption. *IEEE J. Sel. Top. Quantum Electron.* **2001**, *7*, 971−975.

(44) Drobizhev, M.; Meng, F.; Rebane, A.; Stepanenko, Y.; Nickel, E.; Spangler, C. W. Strong Two-Photon Absorption in New Asymmetrically Substituted Porphyrins: Interference between Charge-Transfer and Intermediate-Resonance Pathways. *J. Phys. Chem. B* **2006**, *110*, 9802−9814.

(45) Drobizhev, M.; Karotki, A.; Kruk, M.; Mamardashvili, N. Z.; Rebane, A. Drastic Enhancement of Two-Photon Absorption in Porphyrins Associated with Symmetrical Electron-Accepting Substitution. *Chem. Phys. Lett.* **2002**, *361*, 504−512.

(46) Esipova, T. V.; Vinogradov, S. A. Synthesis of Phosphorescent Asymmetrically π-Extended Porphyrins for Two-Photon Applications. *J. Org. Chem.* **2014**, *79*, 8812−8825.

(47) Karotki, A.; Drobizhev, M.; Kruk, M.; Spangler, C.; Nickel, E.; Mamardashvili, N.; Rebane, A. Enhancement of Two-Photon Absorption in Tetrapyrrolic Compounds. *J. Opt. Soc. Am. B* **2003**, *20*, 321−332.

(48) Biswas, S.; Ahn, H.-Y.; Bondar, M. V.; Belfield, K. D. Two-Photon Absorption Enhancement of Polymer-Templated Porphyrin-Based J-Aggregates. *Langmuir* **2012**, *28*, 1515−1522.

(49) Ogawa, K.; Hasegawa, H.; Inaba, Y.; Kobuke, Y.; Inouye, H.; Kanemitsu, Y.; Kohno, E.; Hirano, T.; Ogura, S.-I.; Okura, I. Water-Soluble Bis(imidazolylporphyrin) Self-Assemblies with Large Two-Photon Absorption Cross Sections as Potential Agents for Photodynamic Therapy. *J. Med. Chem.* **2006**, *49*, 2276−2283.

(50) Ogawa, K.; Ohashi, A. K.; Kobuke, Y.; Kamada, K.; Ohta, K. Two-Photon Absorption Properties of Self-Assemblies of Butadiyne-Linked Bis(Imidazolylporphyrin). *J. Phys. Chem. B* **2005**, *109*, 22003−22012.

(51) Tanihara, J.; Ogawa, K.; Kobuke, Y. Two-photon Absorption Properties of Conjugated Supramolecular Porphyrins with Electron Donor and Acceptor. *J. Photochem. Photobiol., A* **2006**, *178*, 140−149.

(52) Mongin, O.; Sankar, M.; Charlot, M.; Mir, Y.; Blanchard-Desce, M. Strong Enhancement of Two-Photon Absorption Properties in Synergic 'Semi-Disconnected' Multiporphyrin Assemblies Designed for Combined Imaging and Photodynamic Therapy. *Tetrahedron Lett.* **2013**, *54*, 6474−6478.

(53) Drobizhev, M.; Karotki, A.; Kruk, M.; Rebane, A. Resonance Enhancement of Two-Photon Absorption in Porphyrins. *Chem. Phys. Lett.* **2002**, *355*, 175−182.

(54) Humphrey, J. L.; Kuciauskas, D. Charge Transfer Enhances Two-Photon Absorption in Transition Metal Porphyrins. *J. Am. Chem. Soc.* **2006**, *128*, 3902−3903.

(55) Samankumara, L. P.; Zeller, M.; Krause, J. A.; Brückner, C. Syntheses, Structures, Modification, and Optical Properties of *meso*-Tetraaryl-2,3-dimethoxychlorin, and Two Isomeric *meso*-Tetraaryl-2,3,12,13-tetrahydroxybacteriochlorins. *Org. Biomol. Chem.* **2010**, *8*, 1951−1965.

(56) Brückner, C.; Ogikubo, J.; McCarthy, J. R.; Akhigbe, J.; Hyland, M. A.; Daddario, P.; Worlinsky, J. L.; Zeller, M.; Engle, J. T.; Ziegler, C. J.; et al. *meso*-Arylporpholactones and their Reduction Products. *J. Org. Chem.* **2012**, *77*, 6480−6494.

(57) Adler, A. D.; Longo, F. R.; Finarelli, J. D.; Goldmacher, J.; Assour, J.; Korsakoff, L. A Simplified Synthesis for *meso*-Tetraphenylporphine. *J. Org. Chem.* **1967**, *32*, 476−476.

(58) Shima, S.; Ilagan, R. P.; Gillespie, N.; Sommer, B. J.; Hiller, R. G.; Sharples, F. P.; Frank, H. A.; Birge, R. R. Two-Photon and Fluorescence Spectroscopy and the Effect of Environment on the Photochemical Properties of Peridinin in Solution and in the Peridinin-Chlorophyll-Protein from *Amphidinium carterae. J. Phys. Chem. A* **2003**, *107*, 8052−8066.

(59) Kubin, R. F.; Fletcher, A. N. Fluorescence Quantum Yields of Some Rhodamine Dyes. *J. Lumin.* **1983**, *27*, 455−462.

(60) Birge, R. R.; Zhang, C.-F. Two-Photon Double Resonance Spectroscopy of Bacteriorhodopsin. Assignment of the Electronic and Dipolar Properties of the Low-Lying $^1A_g{*}^{-}$−like and $^1B_u{*}^{+}$-like π, π* states. *J. Chem. Phys.* **1990**, *92*, 7178−7195.

(61) Monson, P. R.; McClain, W. M. Polarization Dependence of the Two-Photon Absorption of Tumbling Molecules with Application to Liquid 1-Chloronaphthalene and Benzene. *J. Chem. Phys.* **1970**, *53*, 29−37.

(62) Masthay, M. B.; Findsen, L. A.; Pierce, B. M.; Bocian, D. F.; Lindsey, J. S.; Birge, R. R. A Theoretical Investigation of the One- and Two-Photon Properties of Porphyrins. *J. Chem. Phys.* **1986**, *84*, 3901−3915.

(63) Mortensen, O. S.; Svendsen, E. N. Initial and Final Molecular States as "Virtual States" in Two-Photon Processes. *J. Chem. Phys.* **1981**, *74*, 3185−3189.

(64) Dick, B.; Hohlneicher, G. Importance of Initial and Final States as Intermediate States in Two-Photon Spectroscopy of Polar Molecules. *J. Chem. Phys.* **1982**, *76*, 5755−5760.

(65) Ren, L.; Martin, C. H.; Wise, K. J.; Gillespie, N. B.; Luecke, H.; Lanyi, J. K.; Spudich, J. L.; Birge, R. R. Molecular Mechanism of Spectral Tuning in Sensory Rhodopsin II. *Biochemistry* **2001**, *40*, 13906−13914.

(66) Martin, C. H.; Birge, R. R. Reparameterizing MNDO for Excited State Calculations Using ab Initio Effective Hamiltonian Theory: Application to the 2,4-Pentadien-1-iminium Cation. *J. Phys. Chem. A* **1998**, *102*, 852−860.

(67) Miyahara, T.; Nakatsuji, H.; Hasegawa, J.; Osuka, A.; Aratani, N.; Tsuda, A. Ground and Excited States of Linked and Fused Zinc Porphyrin Dimers: Symmetry Adapted Cluster (SAC) -Configuration Interaction (CI) Study. *J. Chem. Phys.* **2002**, *117*, 11196−11207.

(68) Miyahara, T.; Tokita, Y.; Nakatsuji, H. SAC/SAC-CI Study of the Ground, Excited, and Ionized States of Cytochromes P450CO. *J. Phys. Chem. B* **2001**, *105*, 7341−7352.

(69) Nakajima, T.; Nakatsuji, H. Energy Gradient Method for the Ground, Excited, Ionized, and Electron-Attached States Calculated by the SAC (Symmetry-Adapted Cluster) /SAC-CI (Configuration Interaction) Method. *Chem. Phys.* **1999**, *242*, 177−193.

(70) Nakatsuji, H. Description of Two- and Many-Electron Processes by the SAC-CI Method. *Chem. Phys. Lett.* **1991**, *177*, 331−337.

(71) Foresman, J. B.; Head-Gordon, M.; Pople, J. A.; Frisch, M. J. Toward a Systematic Molecular Orbital Theory for Excited States. *J. Phys. Chem.* **1992**, *96*, 135−149.

(72) Nishimoto, K.; Mataga, N. Electronic Structure and Spectra of Some Nitrogen Heterocycles. *Z. Phys. Chem. (Muenchen, Ger.)* **1957**, *12*, 335−338.

(73) Dewar, M. J. S.; Zoebisch, E. G.; Healy, E. F.; Stewart, J. J. P. Development and Use of Quantum Mechanical Molecular Models. 76. AM1: A New General Purpose Quantum Mechanical Molecular Model. *J. Am. Chem. Soc.* **1985**, *107*, 3902−3909.

(74) Frisch, M. J.; Trucks,, G. W.; Schlegel, H. B.; Scuseria, G. E.; Robb, M. A.; Cheeseman, J. R.; Scalmani, G.; Barone, V.; Mennucci, B.; Petersson, G. A.; et al. *Gaussian 09*, revision D.01; Gaussian, Inc., Wallingford, CT, 2009.

(75) Barone, V.; Cossi, M.; Tomasi, J. Geometry Optimization of Molecular Structures in Solution by the Polarizable Continuum Model. *J. Comput. Chem.* **1998**, *19*, 404−417.

(76) Cossi, M.; Rega, N.; Scalmani, G.; Barone, V. Energies, Structures, and Electronic Properties of Molecules in Solution with the C-PCM Solvation Model. *J. Comput. Chem.* **2003**, *24*, 669−681.

(77) Tomasi, J.; Mennucci, B.; Cammi, R. Quantum Mechanical Continuum Solvation Models. *Chem. Rev.* **2005**, *105*, 2999−3093.

(78) York, D. M.; Karplus, M. Smooth Solvation Potential Based on the Conductor-Like Screening Model. *J. Phys. Chem. A* **1999**, *103*, 11060−11079.

(79) Macak, P.; Luo, Y.; Ågren, H. Simulations of Vibronic Profiles in Two-Photon Absorption. *Chem. Phys. Lett.* **2000**, *330*, 447−456.

(80) Niedzwiedzki, D. M.; Sandberg, D. J.; Cong, H.; Sandberg, M. N.; Gibson, G. N.; Birge, R. R.; Frank, H. A. Ultrafast Time-Resolved Absorption Spectroscopy of Geometric Isomers of Carotenoids. *Chem. Phys.* **2009**, *357*, 4−16.

(81) Chang, J. L. A New Formula to Calculate Franck−Condon Factors for Displaced and Distorted Harmonic Oscillators. *J. Mol. Spectrosc.* **2005**, *232*, 102−104.

(82) Barkigia, K. M.; Thompson, M. A.; Fajer, J.; Pandey, R. K.; Smith, K. M.; Vicente, M. G. H. Conformational Flexibility of Chlorin Macrocycles. Structural Determinations and Theoretical Calculations of a Benzochlorin, a *meso*-Dimethyl Chlorin and a Nickel Chlorin. *New J. Chem.* **1992**, *16*, 599−607.

(83) Senge, M. O.; Hope, H.; Smith, K. M. Structure and Conformation of Photosynthetic Pigments and Related Compounds. Part 6. The First Crystal Structure of a Covalently-Linked Chlorin Dimer: 20,20′-Ethylenebis(trans-2,3,7,8,12,13,17,18-octaethylchlorin). *J. Chem. Soc., Perkin Trans. 2* **1993**, 11−16.

(84) Senge, M. O.; Wiehe, A.; Ryppa, C. Synthesis, Reactivity and Structure of Chlorophylls. *Adv. Photosynth. Respir.* **2006**, *25*, 27−37.

(85) Jentzen, W.; Song, X.-Z.; Shelnutt, J. A. Structural Characterization of Synthetic and Protein-Bound Porphyrins in Terms of the Lowest-Frequency Normal Coordinates of the Macrocycle. *J. Phys. Chem. B* **1997**, *101*, 1684−1699.

(86) Normal-Coordinate Structural Decomposition Engine; http://jasheln.unm.edu/jasheln/content/nsd/NSDengine/start.htm (accessed 1/09/2015) .

(87) Cerussi, A. E.; Berger, A. J.; Bevilacqua, F.; Shah, N.; Jakubowski, D.; Butler, J.; Holcombe, R. F.; Tromberg, B. J. Sources of Absorption and Scattering Contrast for Near-Infrared Optical Mammography. *Acad. Radiol.* **2001**, *8*, 211−218.